# Geochemistry of metamorphosed mafic dikes, Tobacco Root Mountains, southwestern Montana

## Caroline Harris

Department of Geology, Pomona College, 609 N. College Ave., Claremont, CA 91711-6356

*Faculty Sponsor: Richard W. Hazlett, Pomona College*

## INTRODUCTION

Metamorphosed mafic dikes (MMD's) in the Tobacco Root Mountains of southwestern Montana are found in the Indian Creek Metamorphic Suite (ICMS) and Pony Middle Mountain Metamorphic Suite (PMMMS), which are composed largely of quartzofeldspathic and amphibolite gneisses (Fig. 1, Vitaliano et al, 1979). They have not been found in the Spuhler Peak Metamorphic Suite (SPMS), although abundant MMD's have been intruded in the ICMS and PMMMS near their contact with the SPMS. MMD's range from 1/3 - 25m in estimated thickness. Outcrops appear blocky and weathered brown, and exhibit foliation parallel to the margins. In most cases MMD's cross-cut gneiss foliation at low angles, but in some cases dikes are parallel to foliation or cross-cut foliation at high angles. A fresh surface may or may not be foliated, and is typically dark gray in color. Grain sizes range from fine (<1mm) to coarse (>3mm). Minerals visible in hand sample and thin section consist mainly of plagioclase, hornblende, garnet and biotite.

The Tobacco Root Mountains are part of the Wyoming Province, which is believed to represent several amalgamated terranes. The resulting landmass collided with the Superior Province in the early Proterozoic to become the western margin of North America (Wooden et al., 1988). The geochemistry of the MMD's can provide information about the tectonic environment of the terranes in which they were emplaced, thereby constraining formational theories of the Wyoming Province.

## METHODS

Sixty-one MMD samples were collected during the field study. Fifteen of these were analyzed for rare earth, major, and trace elements (REE, major/TEL) using the INAA and XRF facilities at the University of Oregon Radiation Laboratory and Franklin & Marshall College, respectively (Table 1). Thin sections were examined for these samples as well. Samples chosen for analyses are intended to represent MMD distribution throughout the map area; more MMD's from the PMMMS were analyzed than from the ICMS, as the dikes are more abundant in the PMMMS. Samples were also chosen to compare the lithologies of margin vs. core samples, younger versus older dikes, concordant dikes vs. cross-cutting, thinner vs. thicker dikes, dikes containing vs. those not containing garnet, and fine-granied vs. coarse-grained dikes.
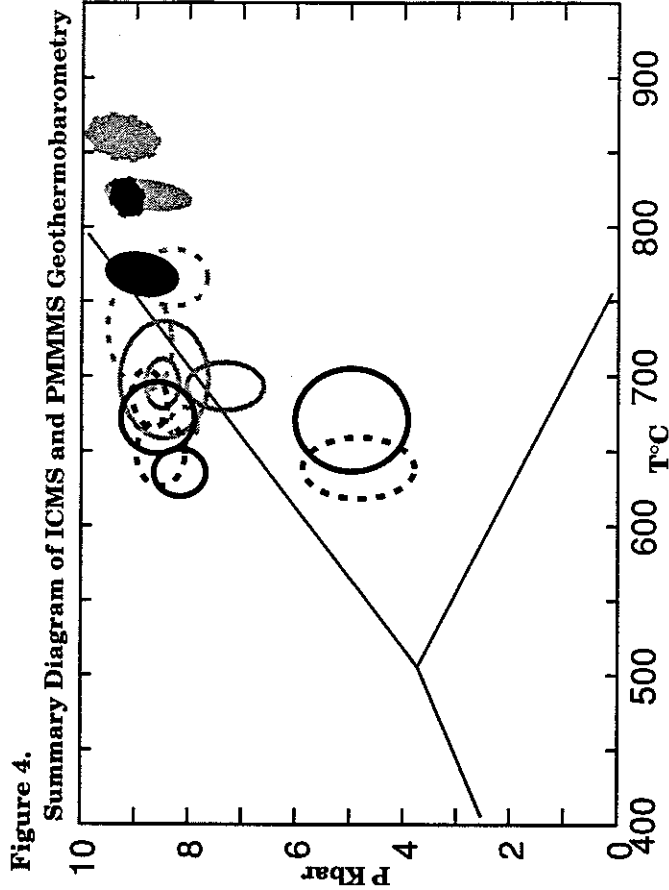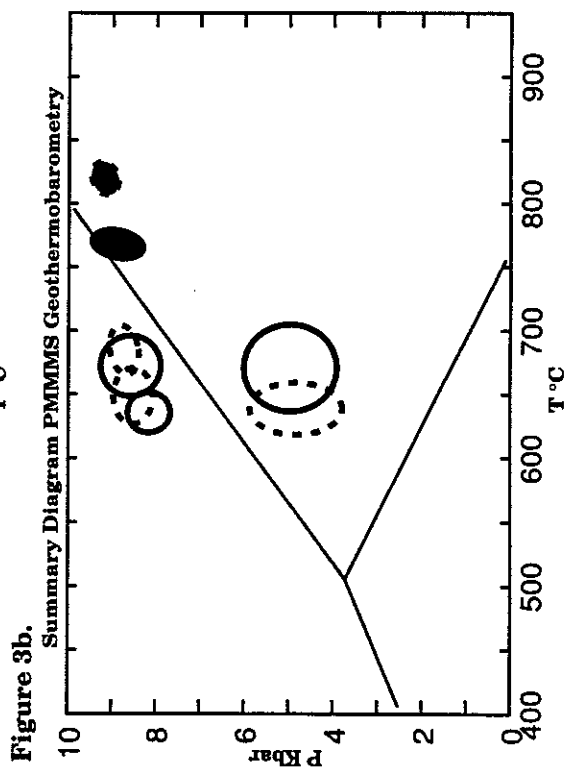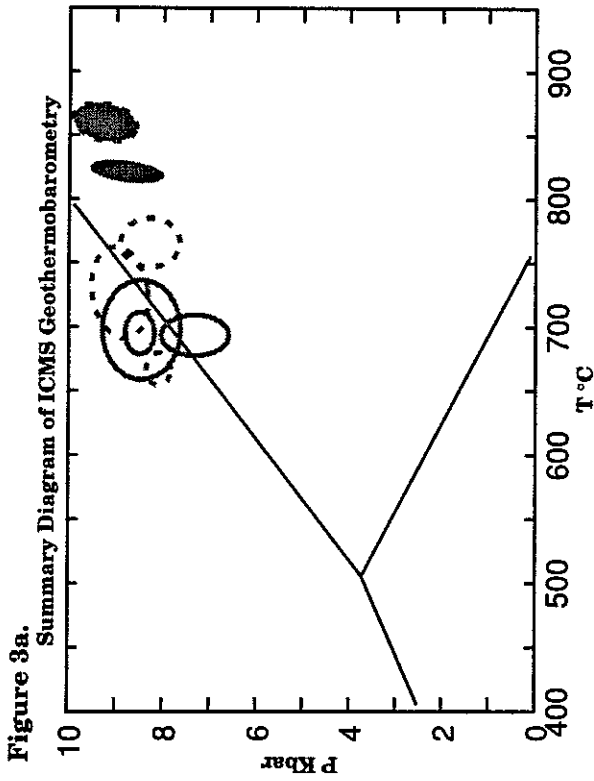
## RESULTS/DISCUSSION

Major element data are considered insufficient to constrain petrogenesis (Wilson, 1989), due to the mobility of major elements in hydrothermal fluids. Hydrothermal alteration is evident in all MMD thin sections by the presence of sericitization and chloritization. Therefore, the mobility of Mn (Rollinson, 1993) and alkali elements should be considered when evaluating the $MnO$-$TiO_2$-$P_2O_5$, $TiO_2$-$K_2O$-$P_2O_5$, and major element discrimination function diagrams (Figs. 1-3). Moreover, the instability of $K_2O$ may influence results in Figure 4.

Trace elements and REEs are considered less mobile and thus are more useful in determining the protolith for altered samples. REEs are relatively immobile even under low-grade metamorphism. However, heavily altered or metamorphosed rocks can cause REE mobility, affecting the accuracy of discrimination graphs (Humphries, 1984).

A spider diagram analysis characteristic of the MMD's exhibits negative anomalies for Sr and Cr (Fig. 5). The light rare earth elements (LREE) and Ba show positive anomalies. Eu remains relatively constant, indicating lack of significant substitution in plagioclase crystallization. The compatibility of Sr in plagioclase (Rollinson, 1993) therefore is an unlikely cause of Sr depletion, since its ionic potential is nearly identical to that of Eu. It is more probable that the negative Sr trend reflects its mobility during leaching (Rollinson, 1993).

Hydrothermal alteration may be the source of anomalous behavior in samples 4-2b and 9-4b in the discrimination diagrams. Both are located near the PMMMS/SPMS contact; juxtaposition of the SPMS may have

Figure 4.
Summary Diagram of ICMS and PMMMS Geothermobarometry

P Kbar

T°C

|  | RIM | INTERIOR |
|---|---|---|
| ICMS | Gt-Hbde Thermometer | Gt-Biot Thermometer |
| PMMMS | Gt-Hbde Thermometer | Gt-Biot Thermometer |
| Gt-Plag-Hbde-Qtz Barometer, no Fe³⁺ Correction | | |

Figure 3a.
Summary Diagram of ICMS Geothermobarometry

P Kbar

T°C

Figure 3b.
Summary Diagram PMMMS Geothermobarometry

P Kbar

T°C

Figure 3c (bottom right). Legend for Figures 3a, 3b, & 4.

175

introduced secondary fluids. Sample 9-4b plots irregularly in the MnO-TiO$_2$-P$_2$O$_5$, discrimination function diagram, Ti-Zr (Fig. 6), and alkali vs. tholeiitic basalt (Fig. 7) diagrams. In the thin section for 9-4b, smaller garnet crystals rim some plagioclase crystals. Other than this characteristic, neither sample 9-4b nor 4-2b are notably distinct from the majority of MMD's in thin section. Sample 4-2b plots distinctly from the other samples in five of the discrimination diagrams. The sample represents a younger, fine grained dike cross-cutting an older dike. Its age could therefore be the cause of its location in the within-plate basalts field in Figure 3, possibly affected by crustal contamination rather than proximity to the SPMS. Moreover, other samples near the SPMS contact lie within volcanic arc fields in the diagrams.

Ba is regarded as a relatively mobile element (Rollinson, 1993), and its positive trend in the spider diagram represents Ba enrichment in the source. Enrichment behavior is often the result of fluids added during subduction processes (Rollinson, 1993). Typical Archean packages in which mafic dikes are emplaced have undergone amphibolite to granulite grade metamorphism (Windley, 1984); although granulite facies are depleted in elements that could contaminate basalt, the Ba anomaly could indicate crustal contamination (Condie et al., 1987). Hole et al. (1984) suggest that subducted sediments cause Ba enrichment, creating this trend in island-arc basalts.

Major element diagrams suggest an island-arc tholeiite environment for MMD intrusion. MMD samples plot as tholeiitic basalts (Fig. 7), and represent an oceanic environment, according to the TiO$_2$-K$_2$0-P$_2$O$_5$ discrimination diagram for basalts. Samples primarily plot in the calc-alkali basalt and island arc tholeiite field in the discrimination function diagram. The MnO-TiO$_2$-P$_2$O$_5$ diagram narrows this field to suggest a pure island-arc tholeiite environment. One sample, 2-4, plots anomalously in three of the discrimination diagrams. However, sample 2-4 is not an MMDS; the main indicator of this is the lack of garnet in thin section.

Trace element behavior also classifies the MMD's as volcanic-arc basalts in the Th-Hf-Ta diagram (Fig. 8). However, all but one sample plotted in this field lie outside of the island-arc tholeiite range. These results represent enrichment of Th, a mobile element in altered basalts (Rollinson, 1993).

The trend toward the K$_2$0 corner of Figure 2 similarly can be attributed to K$_2$0 mobility, and causes several MMD's to plot as continental tholeiites. K$_2$0 mobility should cause its enrichment in volcanic arcs, as it is assimilated into basalts during ascension through granitic crust (Richard Hazlett, pers. commun., 1998). However, MMD's plot as low K$_2$0/Yb ratios in Figure 4. If MMD's represent an accretionary wedge in the forearc environment, as suggested by Wilson and Hyndman (1990), the dikes would have ascended through very little crust, and K$_2$0 concentrations would not be particularly enriched.

Unique conditions in the Archean may not be accurately represented by the discrimination diagrams used in this study, which are modeled after current geothermal conditions and tectonic processes. The geothermal gradient was higher in the Archean than at present (Windley, 1984). According to Windley (1984), heat was lost through convection by a faster subduction rate under a thinner lithosphere. Nevertheless, the data seem to suggest emplacement of the dikes in a primitive island arc oceanic environment. The results are consistent with the hypothesis that the Tobacco Root Mountains represent an accreted forearc basin (Wilson and Hyndman (1990).

## ACKNOWLEDGMENTS

## REFERENCES

Burger, H. Robert, Brady, John B., Cheney, John T., Harms, Tekla A., Johnson, Kathleen E., 1995, Geochemistry, petrology, and structure of Archean rocks, Tobacco Root Mountains, southwestern Montana: Eighth Keck Research Symposium in Geology, p. 69.

Condie, Kent C., Bobrow, D.J., Card, K.D., 1985, Geochemistry of Precambrian mafic dykes from the southern Superior Province of the Canadian Shield: GSA Special Paper 34, p. 95-108.

Hole, J. J., Saunders, A. D., Marriner, G. F. and Tarney, J., 1984, Subduction of pelagic sediments: implications for the origin Ce-anomalous basalts from the Mariana Islands: J. Geol. Soc. Lond., v. 141, p. 453-472.

Humphries, S.E., 1984, The mobility of the rare earth elements in the crust, In: Henderson P. (Ed.), Rare earth geochemistry: Elsevier, Amsterdam, p. 315-341.

Mullen, E.D., 1983, MnO/TiO$_2$/P$_2$O$_5$: a minor element discriminant for basaltic rocks of oceanic environments and its implications for petrogenesis: Earth Planet. Sci. Lett., v. 62, 53-62.

Pearce, J.A., 1976, Statistical analysis of major element patterns in basalts: J. Petrol., v. 17, 15-43.

Pearce, J.A., 1982, Trace element characteristics of lavas from destructive plate boundaries, in: Thorpe R.S. (ed.): Andesites, Wiley, Chichester, pp. 525-548.

Pearce, T.H., Gorman, B.E. and Birkett, T.C., 1975, The $TiO_2$-$K_2O$-$P_2O_5$ diagram: a method of discriminating between oceanic and non-oceanic basalts: Earth Planet. Sci. Lett., v. 24, 419-426.

Rollinson, Hugh R., 1993, Using geochemical data: evaluation, presentation, interpretation: Essex, England, Longman Scientific & Technical.

Vitaliano, C. J. And Cordua, W. S., 1979, Geologic map of the southern Tobacco Root Mountains, Madison County, Montana: Geol. Soc. Of America, map MC-31.

Wilson, Marjorie, 1989, Igneous petrogenesis: London, Unwin Hyman Ltd.

Wilson, Michael L. and Hyndman, Donald W., 1990, Tectonic Interpretation of an Archean lithologic package enclosing iron-formation in the southern Tobacco Root and Northern Ruby Ranges of southwestern Montana, USA, in Chauvel, J. J. et al, eds., Ancient Banded Iron Formations: Athens, Theophrastus Publications, p. 27-61.

Winchester, J.A. and Floyd, P.A., 1976, Geochemical magma type discrimination; application to altered and metamorphosed basic igneous rocks: Earth Planet. Sci. Lett., v. 28, 459-469.

Windley, Brian F., The evolving continents: John Wiley & Sons, New York.

Wood, D.A., 1980, The application of a Th-Hf-Ta diagram to problems of tectonomagmatic classification and to establishing the nature of crustal contamination of basaltic lavas of the British Tertiary volcanic province: Earth Planet. Sci. Ett., v. 50, 11-30.

Wooden, J. L., Mueller, P. A., and Mogk, D. W., 1988, A review of the geochemistry and geochronology of the Archean rocks of the northern part of the Wyoming province, in Ernst, W., ed., Metamorphism and crustal evolution in the western U. S.: Rubey Volume, v. VII New York, Prentice-Hall, p. 383-410.

| TABLE 1 | | | | | | | | | | |
|---|---|---|---|---|---|---|---|---|---|---|
| MAJOR OXIDES * | | TRACE/REE * | | | | | | | | |
| (mean +/- standard dev.) | | (mean +/- standard dev.) | | | | | | | | |
| SiO2 (%) | 50.04 +/- 0.96 | La (ppm) | 10.54 +/- 6.27 | U (ppm) | 0.80 +/- 0.39 | | | Zr (ppm) | 116.92 +/- 61.54 | |
| TiO2 (%) | 1.39 +/- 0.58 | Ce (ppm) | 24.59 +/- 13.01 | Sc (ppm) | 41.18 +/- 10.00 | | | As (ppm) | 2.13 +/- 1.16 | |
| Al2O3 (%) | 13.36+/- 0.79 | Nd (ppm) | 14.99 +/- 7.20 | Cr (ppm) | 142.17 +/- 69.12 | | | Sb (ppm) | 0.22 +/- 0.35 | |
| FeO (%) | 11.34 +/- 2.47 | Sm (ppm) | 3.73 +/- 1.64 | Co (ppm) | 50.49 +/- 14.25 | | | Se (ppm) | 1.60 +/- 0.34 | |
| MnO (%) | 0.24+/- 0.20 | Eu (ppm) | 1.24 +/- 0.46 | Rb (ppm) | 24.24 +/- 15.53 | | | W (ppm) | 1.46 +/- 0.91 | |
| MgO (%) | 6.11 +/- 0.80 | Tb (ppm) | 0.76 +/- 0.20 | Cs (ppm) | 1.39 +/- 1.93 | | | Hg (ppm) | 0.04 +/- 0.01 | |
| CaO (%) | 10.40 +/- 0.68 | Yb (ppm) | 2.76 +/- 0.45 | Ba (ppm) | 215.07 +/- 177.48 | | | Au (ppb) | 0.01 +/- 0.0 | |
| Na2O (%) | 1.97 +/- 0.16 | Lu (ppm) | 0.34 +/- .08 | Ni (ppm) | 148.64 +/- 66.46 | | | Ir (ppb) | 0.01 +/- 0.02 | |
| K2O (%) | 0.48 +/- 0.18 | Hf (ppm) | 3.32 +/- 2.42 | Sr (ppm) | 173.14 +/- 63.77 | | | Os (ppb) | 0.96 +/- 0.96 | |
| P2O5 (%) | 0.13 +/- 0.07 | Ta (ppm) | 0.50 +/- 0.34 | V (ppm) | 284.79 +/- 44.49 | | | | | |
| | | Th (ppm) | 2.32 +/- 2.70 | Zn (ppm) | 123.71 +/- 23.64 | | | | | |
| * sample 2-4 excluded | | | | | | | | | | |
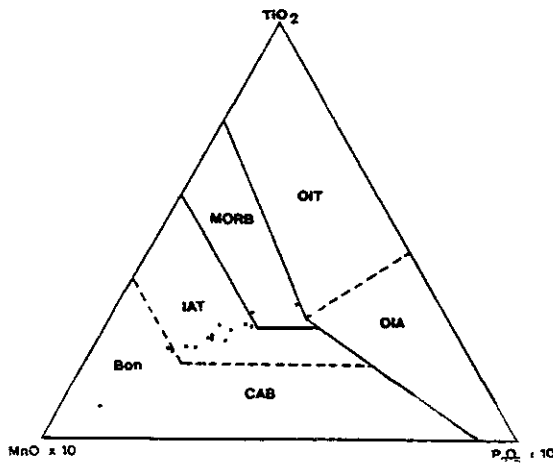


Figure 1. MnO-$TiO_2$-$P_2O_5$ discrimination diagram for basalts and basaltic andesites (45-54 wt% $SiO_2$) (after Mullen, 1983). OIT: ocean-island tholeiite/seamount toleiite; OIA : ocean-island alkali basalt/seamount alkali basalt; CAB: island-arc calc-alkaline basalt; IAT: island-arc tholeiite; Bon: boninite.
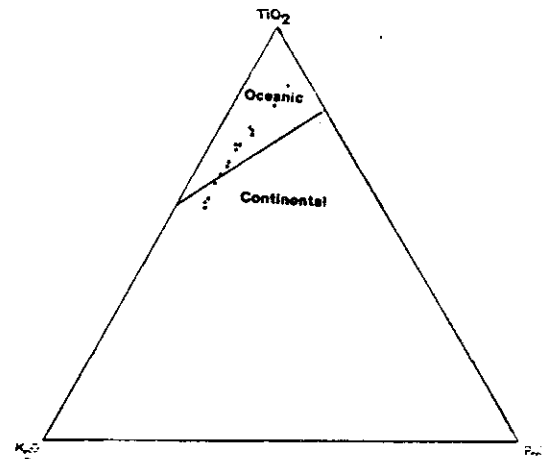


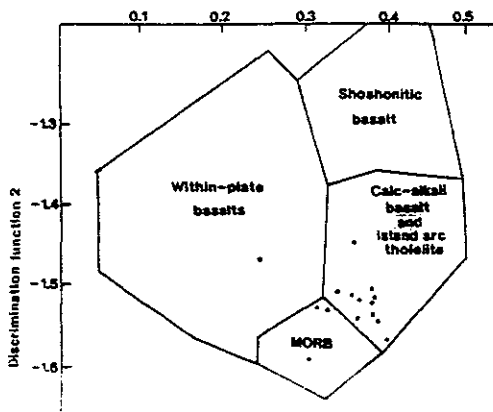Figure 2. $TiO_2$-$K_2O$-$P_2O_5$ discrimination diagram for basalts (after Pearce et al., 1975).

178

Figure 3. Major element discrimination diagram for basalts (after Pearce, 1976). Function 1: +0.0088SiO$_2$ - 0.0774TiO$_2$ + 0.0102Al$_2$O$_3$ + 0.0066FeO - 0.0017MgO - 0.0143CaO - 0.0155Na$_2$O - 0.0007K$_2$O. Function 2: - 0.0130SiO$_2$ - 0.0185TiO$_2$ - 0.0129Al$_2$O$_3$ - 0.0134FeO - 0.0300MgO - 0.0204CaO - 0.0481Na$_2$O - 0.0715K$_2$O.
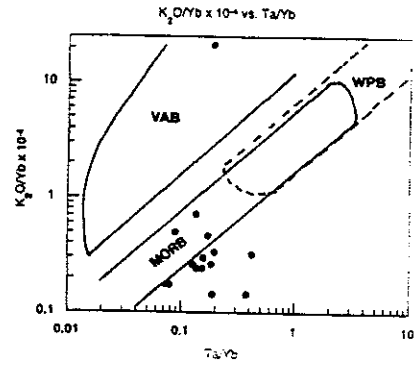


Figure 4. Basalt discrimination diagram (simplified), using Yb as a normalizing factor (after Pearce, 1982). VAB: volcanic-arc basalts; WPB: within-plate basalts.
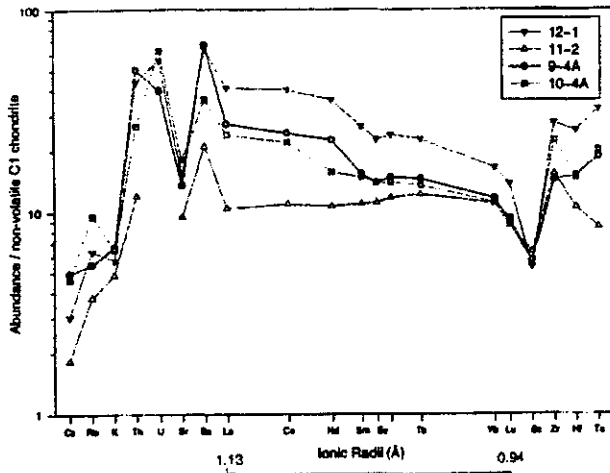


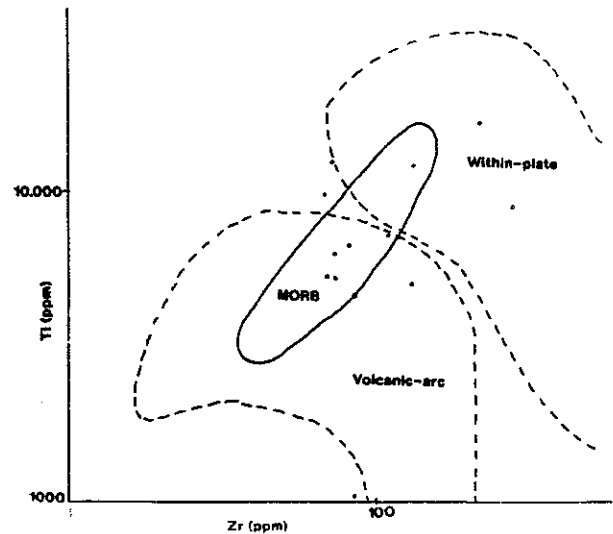Figure 5. Spider diagram for four MMD samples. Courtesy of Oregon State University Radiation Center.



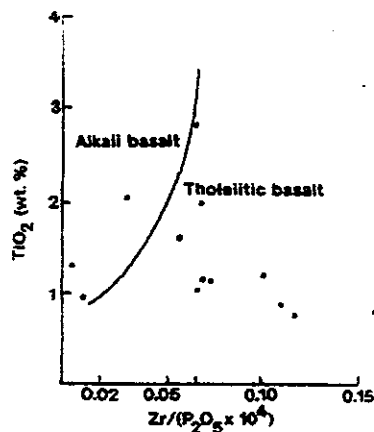Figure 6. Ti-Zr basalt discrimination diagram (after Pearce and Cann, 1973).



Figure 7. TiO$_2$-Zr/ (P$_2$O$_5$ x 10$^M$) basalt discrimination diagram (after Winchester and Floyd, 1976).
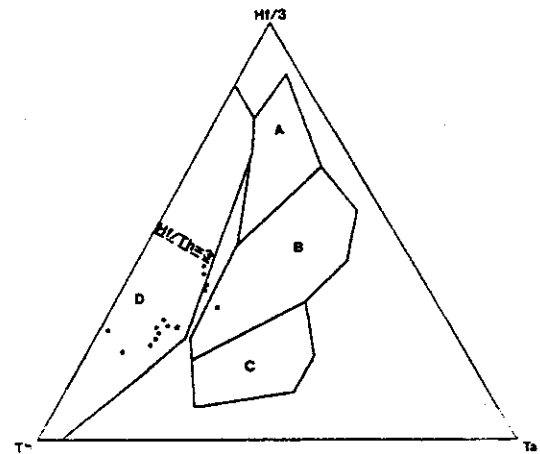


Figure 8. Th-Hf-Ta discrimination diagram for basalts (after Wood, 1980). A: N-type MORB; B: E-type MCRB and within-plate tholeiites; C: alkaline within-plate basalts; D: volcanic-arc basalts, with island-arc tholeiites plotting in the field where Hf/Th > 3.0.

179

# Sapphirine symplectites in orthoamphibolites of the Archean Indian Creek Metamorphic Suite (ICMS), Tobacco Root Mountains, Montana

## Christine E. Hatch

Department of Geology, Amherst College, Amherst, MA 01002-5000
*Faculty sponsor: John T. Cheney, Amherst College*

## INTRODUCTION

The ICMS is one of three metamorphic suites that comprise the Archean rocks in the Tobacco Root Mountains. As described by Burger et al. (1994), the ICMS represents metasupracrustal rocks whose protoliths are a sequence of marine sedimentary rocks with possible interlayered volcanics or felsic intrusives. ICMS lithologies include quartzo-feldspathic and hornblende gneisses, marble, schists, quartzite, iron formation and minor orthoamphibole gneiss.

Due to their structural and petrographical similarities, the ICMS and the Pony Middle Mountain Metamorphic Suite (PMMMS) have been interpreted to be the same unit which was later juxtaposed with the Spuhler Peak Metamorphic Suite (SPMS) during distributed simple shear (Harms et al., 1996). Previous petrologic studies on SPMS rocks summarized by Cheney et al. (1994, 1996) have shown that the SPMS is polymetamorphic and involves an earlier high pressure (>10kb.) event followed by a later lower pressure (<6kb.) event. This last event was amphibolite to granulite facies in grade and had T's and P's of 650 ± 25 °C and 5.5 ± 1kb., and corresponds to $^{40}Ar/^{39}Ar$ hornblende ages of 1800 Ma, and a clockwise P-T-t path.

## PURPOSE AND METHODS

Samples were taken from various sites within the ICMS, with particular interest paid to amphibolite gneisses containing orthopyroxene. Detailed analysis has been focused primarily on two main areas: "Quartz Creek", the ridgeline running from Leggat Mountain south toward Quartz Creek, and "Granite Creek", an area just inside the Beaverhead National Forest boundary near the east fork of Granite Creek on the southeastern flank of the range. These areas contain the most interesting and varied lithologies that provide the most information with which to constrain the tectonometamorphic evolution of the ICMS.

## PETROGRAPHY

This study focuses on an orthoamphibolite lithology found in both the Quartz Creek and Granite Creek areas. This assemblage consists of garnet + orthoamphibole + orthopyroxene ± biotite ± rutile + quartz, with some variations, including kyanite and staurolite inclusions in the garnets, ± kyanite or sillimanite, and ± cordierite. Two reaction textures are present in Granite Creek rocks: a cordierite + orthopyroxene symplectite, and a sapphirine + spinel + cordierite symplectite.

## DISCUSSION

Documentation of the previous history of the ICMS has been somewhat ambiguous and self-contradictory. Brady et al. (1994) reported a counter-clockwise P-T path in the ICMS based on aluminous schist minerology. Tuit (1996) agreed based on the occurence of garnet rims (with Cpx and Plag) on Opx porphyblasts in amphibolites, and garnet zoning in pelitic schists. However, Cheney et al. (1996) claimed that geothermobarometry from ICMS amphibolites is consistant with the (clockwise P-T-t path) evolution of the SPMS.

The cordierite + orthopyroxene symplectite observed in the ICMS Granite Creek rocks (see figure 2a-c) represents the rapid mineral growth as garnet is consumed in the following reaction:

garnet + quartz --------> cordierite + orthopyroxene
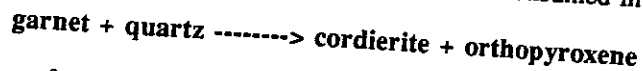
$$(1)$$

This type of symplectite has been interpreted as indicative of decompression (or a clockwise P-T-t path) by Raith (1997). This observation agrees with Cheney (1996), and is consistant with the texture in hornblende amphibolites near Quartz Creek also cited by Tuit (1996), consisting of garnet rims on orthopyroxene. According to Spear (1997) for rocks with similar textures and grade in the Adirondack mountains of New York, garnet rims of this type can grow during cooling as part of a clockwise P-T-t path.

Another symplectic assemblage found in the Granite Creek area also represents rapid mineral growth. The sapphirine + spinel + cordierite symplectite (see figure 3a-c) represents a local quartz-absent